Available online at www.sciencedirect.com
SCIENCE DIRECT®
Journal of the European Ceramic Society 25 (2005) 1905–1918
www.elsevier.com/locate/jeurceramsoc

Effects of TiO_2 and SiO_2 additions on phase formation, microstructures and PTCR characteristics of Sb-doped barium strontium titanate ceramics

P. Bomlai[a,b,*], N. Sirikulrat[a], A. Brown[b], S.J. Milne[b]

[a] *Department of Physics, Faculty of Science, Chiang Mai University, Chiang Mai 50200, Thailand*
[b] *Institute for Materials Research, University of Leeds, Leeds LS2 9JT, UK*

Received 19 February 2004; received in revised form 26 May 2004; accepted 4 June 2004
Available online 12 August 2004

Abstract

Phase formation, densification, microstructural development and the electrical resistivity of Sb-doped $Ba_{0.8}Sr_{0.2}TiO_3$ ceramics, containing different sintering additives have been investigated. A secondary phase of $(Ba_{1-x}Sr_x)_6Ti_{17}O_{40}$ was found in samples containing 1 mol% excess TiO_2, whereas in samples containing a combination of 1 mol% TiO_2 and 3 mol% SiO_2 an additional fresnoite solid solution phase, $Ba_{1-y}Sr_yTi_{1+x}Si_{2-x}O_8$, was found to co-exist at intergranular regions. Grain growth was suppressed by the single TiO_2 additive, but no improvement in densification was observed. However, the combined excess of SiO_2 and TiO_2 promoted liquid phase sintering, producing a reduction in sintering temperature from ~1350 °C to ~1250 °C; this additive combination also enhanced the PTCR response.

Keywords: (Ba,Sr)TiO_3; PTCR ceramics; Sintering aids; Phase analysis

1. Introduction

Ceramics exhibiting a positive temperature coefficient of resistivity (PTCR) are used in a wide variety of applications, such as over-current protection, self-regulating heaters, and temperature sensors.[1] Low resistivity at room temperature and a strong PTCR effect are both critical parameters for device applications. Barium titanate, $BaTiO_3$, is the basis for most PTCR materials, however, unmodified $BaTiO_3$ is an insulator which shows a high intrinsic resistivity of more than 10 Ω^{10} cm at room temperature, when prepared in an oxidizing atmosphere, and no PTCR effect can be observed.[2] The desired semiconducting $BaTiO_3$ phase, exhibiting a non-linear change of resistivity with temperature, can be achieved by donor doping, coupled to careful selection of heat-treatment conditions to control the interaction of the grain boundaries with oxygen during ceramic fabrication.[3] Examples of donor additives are trivalent ions (e.g. La^{3+}, Sb^{3+}) substituting on Ba^{2+} sites, or pentavalent ions (e.g. Nb^{5+}, Ta^{5+}) substituting on Ti^{4+} sites of the perovskite ABO_3 lattice.[1]

Heywang first proposed that the PTCR effect was dependent on electron traps (acceptor states) along grain boundaries resulting in electron depletion layers and Schottky barriers.[4] Jonker subsequently explained the absence of any PTCR effect below the Curie temperature (T_C) in terms of spontaneous polarisation of ferroelectric domains.[5] The overall resistance of the sample is dependent on the resistance of the grain boundary regions, the value being affected by interaction with oxygen and changes to the density of acceptor states during processing. A maximum resistance is reached at T_{max}, due to the increasing energy levels of electron traps. Dopant type and concentration, processing conditions and oxygen partial pressures all influence the PTCR effect.[6,7]

Solid solutions of $BaTiO_3$ with $SrTiO_3$ ($Ba_{1-x}Sr_xTiO_3$) are particularly useful for PTCR applications since the Curie temperature can be varied by changing the Ba/Sr ratio, which offers flexibility in controlling the temperature range over which the PTCR effect can be utilised.[8,9]

* Corresponding author. Tel.: +66 53 943 376; fax: +66 53 357 512.
E-mail address: ppornsuda@yahoo.com (P. Bomlai).

0955-2219/$ – see front matter © 2004 Elsevier Ltd. All rights reserved.
doi:10.1016/j.jeurceramsoc.2004.06.015

It is common practice in electroceramic fabrication to introduce various additives to control microstructures and to enhance densification at reduced sintering temperatures. For example, in $BaTiO_3$ processing, a small excess of TiO_2 is often added to produce a composition with a relatively low solidus temperature, ~1330 °C, which promotes liquid phase sintering and densification at lower temperatures than in unmodified $BaTiO_3$.[10] The sintering temperature of $BaTiO_3$ may also be reduced by adding SiO_2, which reportedly gives a solidus temperature of ~1260 °C.[11,12] More complex additive compositions are also used, for example, a mixed alumina silica titania system (AST), is reported to reduce sintering temperatures and enhance the PTCR effect in $BaTiO_3$.[13] The AST additive has also been added to BST to induce liquid phase sintering.[14,15]

It was originally suggested that AST improved PTCR properties by providing a liquid which acts as a grain boundary 'chemical sink' for impurities that otherwise would degrade the PTCR effect; microstructural changes associated with liquid phase sintering are also likely to be important. Recently it has been suggested that cooling rates in BST–AST systems affect the PTCR response due to changes in the thickness of a BST phase precipitated from the liquid onto BST matrix grains during cooling; enhancements in the PTCR effect were thought to be due to consequent changes in the acceptor state density and the polarisation state at grain boundaries[14] stemming from the 'acceptor-rich' liquid.

In order to provide further information on the role of sintering additives in donor-doped BST ceramics we have examined the effects on microstructures and PTCR responses of additive systems which do not include Al^{3+} (which is a possible acceptor dopant on Ti sites). One was a single TiO_2 additive (1 mol%), the other a combination of TiO_2 (1 mol%) and SiO_2 (3 mol%); both of these systems induce liquid phase sintering in ceramics of the parent $BaTiO_3$ composition. The additives were added to a standard Sb-doped $Ba_{0.8}Sr_{0.2}TiO_3$ PTCR composition.[15,16] Particular attention was given to examining the effect of the additives on intergranular phases formed on cooling the liquid.

2. Experimental procedure

Ceramic samples were prepared by the conventional mixed oxide process. The starting powders of $BaCO_3$, TiO_2, $SrCO_3$, Sb_2O_3, SiO_2 (Aldrich chemical company, Inc., 99.9+% purity) were used to prepare the compositions shown in the following, in which Sb^{3+} substitution on the Ba^{2+} site is assumed.

Composition 1: $(Ba_{0.797}Sr_{0.2})Sb_{0.003}TiO_3$ (Sb-BST)
Composition 2: Sb-BST + 1 mol% TiO_2 (Sb-BST + TiO_2)
Composition 3: Sb-BST + 1 mol% TiO_2 + 3 mol% SiO_2 (Sb-BST + TiO_2/SiO_2)

There is debate as to the charge compensation mechanism(s) in donor-doped perovskites involving substitution of trivalent ions, of suitable ionic radii, on the A sites of the ABO_3 lattice. Possible mechanisms include Ti vacancy formation, Ba/Sr vacancy formation, or electronic compensation.[6,7] In the present work Sb-BST was made by simple additions of Sb_2O_3 (0.15 mol%) with a 1:1 compensation of the A sites and no reduction in the TiO_2 content. The possible consequences of this on solid solution formation and the phases produced during sintering are discussed later in the text.

The mixed powders were ball milled with zirconia grinding media in isopropanol for 20 h, then dried and sieved, followed by calcination at 1000 °C for 3 h in an alumina crucible, using heating and cooling rates of 5 °C/min. In order to obtain compacted pellets, the calcined powders were blended with 1% PVA and ball-milled for 6 h, dried and sieved again before pressing into 1.5 cm diameter pellets at 100 MPa. For binder removal, samples were heated at a rate of 2 °C/min, and held at 500 °C for 1 h. The samples were then sintered in air at various temperatures ranging from 1200 °C to 1450 °C, for 1 h, using heating and cooling rates of 5 °C/min.

Phase identification of powders and sintered samples was carried out at room temperature using an X-ray powder diffraction technique (XRD) with a scan speed of 0.004°/s, using Cu Kα radiation (Philips APD1700). The density of sintered samples was obtained by geometric measurements. The microstructures of the as-sintered surfaces were observed using scanning electron microscopy (ESEM, Phillips XL30). Backscattered imaging and X-ray mapping were carried out to monitor the distributions of each phase in the microstructure (Camscan series 4 SEM, with Oxford Instruments UTW EDX detector/ ISIS software series 300 for microanalysis and digital image capture). Transmission electron microscopy was also employed (Philips CM20 TEM, with Oxford Instruments EDX facility). Samples for TEM examination were cut into 3 mm disks, mechanically ground to 300 μm, 'dimpled' to a thickness of ~30 μm, and finally Ar^+-ion beam milled down to perforation for electron transparency. The dc resistance change of the specimens as a function of temperature was measured using a digital multimeter (Agilent 34401A) and a suitable power supply; electrodes were applied using silver paste. The measurements were carried out from room temperature to ~300 °C using a silicone oil bath to heat the samples; a digital thermometer (Fluke S50) with a K-type thermocouple was used to monitor temperature.

3. Results

The XRD patterns for powders of each of the three compositions, calcined at 1000 °C for 3 h, are shown in Fig. 1. At room temperature the parent composition, $Ba_{0.8}Sr_{0.2}TiO_3$ should be tetragonal with a c/a lattice parameter ratio of 1.003.[17] However, no tetragonal peak splitting was evident in any of the Sb-BST powder samples (even at angles up to 90° 2θ). This was probably due to peak broadening effects caused by chemical inhomogeneities in the powder mixture, and in-

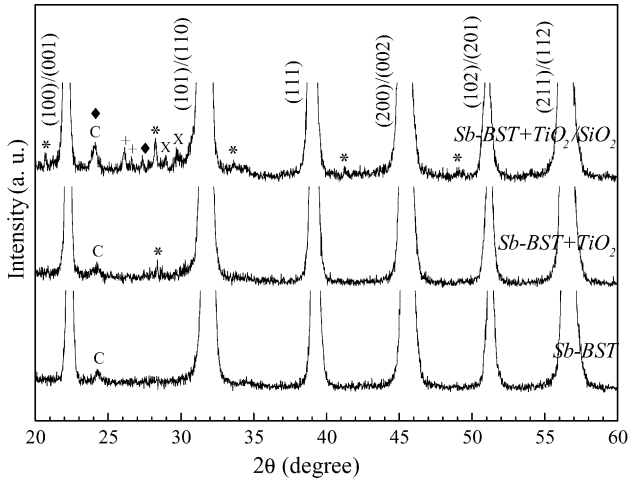

Fig. 1. X-ray diffraction patterns of powders showing phase formation with different additives when calcined at 1000 °C for 3 h ((*) $Ba_4Ti_{13}O_{30}$, (♦) $Ba_5SrSi_{10}O_{26}$, (+) β-$BaSiO_3$, X: $Ba_4Ti_{11}O_{26}$ and C: $BaCO_3$).

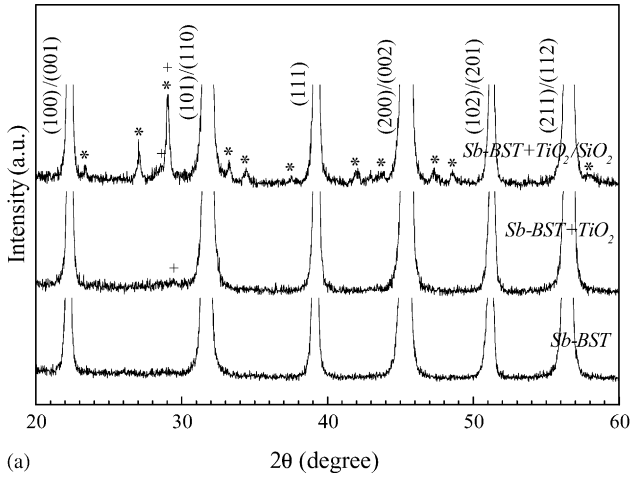

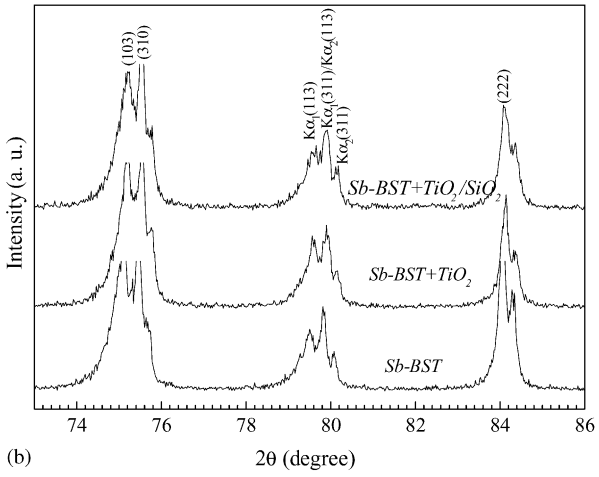

Fig. 2. (a) X-ray diffraction patterns of samples sintered at 1400 °C showing phase formation with different additives ((*) $Ba_2TiSi_2O_8$ and (+) $Ba_6Ti_{17}O_{40}$). (b) X-ray diffraction patterns of samples sintered at 1400 °C showing tetragonal peak splitting of the high angle peaks.

complete solid state reaction during calcination (crystallite size effects are unlikely after high temperature calcination). The resultant localized variations in solid solution composition (Ba:Sr ratio) would give a variety of slightly different lattice parameters, and broadened XRD peaks. All three calcined powder compositions showed an extra peak at 24.2° 2θ suggesting the presence of a barium carbonate phase.[18] This was either a result of incomplete decomposition of the starting carbonate, or due to carbonation of the calcined powder after standing in air. Powders of composition 2 (excess TiO_2) showed evidence of a faint diffraction peak similar in position to that of the most intense reflection of $Ba_4Ti_{13}O_{30}$.[19] For powders of composition 3 (excess TiO_2 + SiO_2), numerous faint XRD peaks were evident (Fig. 1). Comparisons with standard XRD files suggested these represented a complex secondary phase mixture of: $Ba_5SrSi_{10}O_{26}$,[20] β-$BaSiO_3$,[21] $Ba_4Ti_{13}O_{30}$[19] and $Ba_4Ti_{11}O_{26}$,[22] as labelled in Fig. 1. Partial substitution of Sr for Ba may have occurred in some of these phases.

In the sintered ceramics, Fig. 2(a), XRD peaks of the main phase became sharper, indicating improved compositional uniformity of the BST solid solution; the carbonate peaks had disappeared at these higher temperatures. Tetragonal peak splitting was now evident at high angles (in addition to splitting due to the separation of Kα_1 and Kα_2 peaks). The example of the 1 1 3/3 1 1 peaks at ∼80° 2θ is shown in Fig. 2(b). The values of a and c lattice parameters were estimated using a manual least square fitting method;[23] all samples gave similar average values, a = 3.97 ± 0.05 Å and c = 3.99 ± 0.05 Å, giving a c/a ratio of 1.01 ± 0.05.

Sintered ceramics of composition 2 (excess TiO_2) possessed one faint additional peak at an angle corresponding to the main peak in the standard pattern of $Ba_6Ti_{17}O_{40}$, at 29.16° 2θ,[24] Fig. 2(a); this phase is referred to as the 6:17 phase. In the case of composition 3, the 6:17 phase was again present but there were a number of other extra peaks, which comparisons with standard patterns indicated to be similar in d-spacings to $Ba_2TiSi_2O_8$,[25] referred to as the 2:1:2 phase, Fig. 2(a), The other secondary phases previously present in the calcined powder of composition 3 were no longer present in the sintered samples.

The geometric densities of sintered samples prepared at various sintering temperatures are shown in Fig. 3. For compositions 1 and 2, density increased sharply between sintering temperatures of 1300 °C and 1350 °C, but with little subsequent change up to 1450 °C. For composition 3, densification occurred at lower temperatures than for the other two samples, reaching a maximum density at ∼1250 °C, but then declining slightly with further increments in sintering temperature. The lower densification temperature of composition 3 was consistent with the added TiO_2 + SiO_2 producing a liquid phase during sintering at 1250 °C, which aided densification. The fall off in density at higher temperatures may be due to greater amounts of liquid being produced, from which an increasing amount of the lower density 2:1:2 silicate

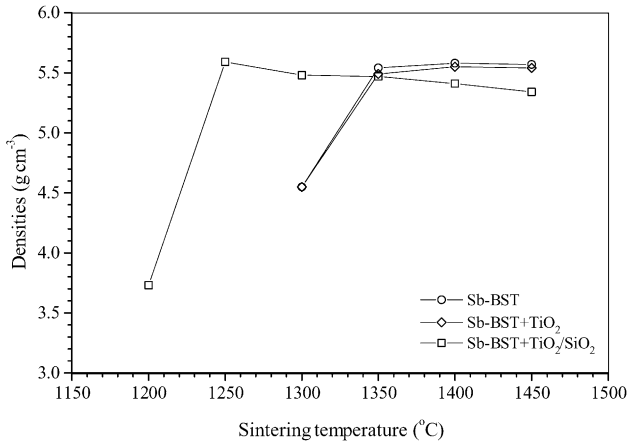

Fig. 3. The densities (geometric) of sintered samples as a function of sintering temperatures and additives.

phase, and the 6:17 phase, crystallized. The reported densities of $Ba_6Ti_{17}O_{40}$ and $Ba_2TiSi_2O_8$ phases are 4.79 g cm^{-3} and 4.42 g cm^{-3}, respectively,[24,25] compared to a value of 5.84 g cm^{-3} for Sb-BST calculated from the experimental lattice parameter measurements obtained from XRD data. There may also have been some unidentified low density glassy phase present in the samples after cooling.

The 6:17 second phase was present in only very low amounts in sintered ceramics of composition 2 (Fig. 2) and therefore a value of 5.84 g cm^{-3} is probably a reasonable estimate of theoretical density for both compositions 1 and 2. This gave a percentage theoretical density value of ∼95% for ceramics of both compositions sintered at ≥1350 °C. For composition 3, from XRD there was a greater amount of crystalline secondary phases (mainly 2:1:2 plus some 6:17), and as the proportion of these was not known, an estimate of a limiting density in terms of a percentage is less meaningful.

Compositions 1 and 2 after sintering at 1350 °C each displayed similar microstructures, with a bimodal grain size distribution of large grains in a fine-grained matrix, Fig. 4(a). This type of secondary, or exaggerated, grain growth is characteristic of $BaTiO_3$ and related compositions.[26] The coarsened grains were ≤40 μm in size for Sb-BST, but this decreased to ≤30 μm for the sample with 1 mol% of added TiO_2. After sintering at 1400 °C, the larger secondary grains extended throughout the microstructure and the bimodal distribution disappeared, Fig. 4(b). There was only a slight increase in grain size on raising the sintering temperature from 1400 °C to 1450 °C, for the TiO_2 modified sample (composition 2), but without the TiO_2 addition (composition 1), the maximum grain sizes increased from ∼40 μm to ∼60 μm.

Composition 3 produced a different microstructure. No secondary grain growth was apparent at any temperature studied (in the range 1200–1450 °C); an example sintered at 1350 °C is shown in Fig. 4(c). Instead many grains were rounded in form, consistent with the addition of SiO_2 + TiO_2 producing a liquid phase at the sintering temperatures (as already implied by the lower densification temperature,

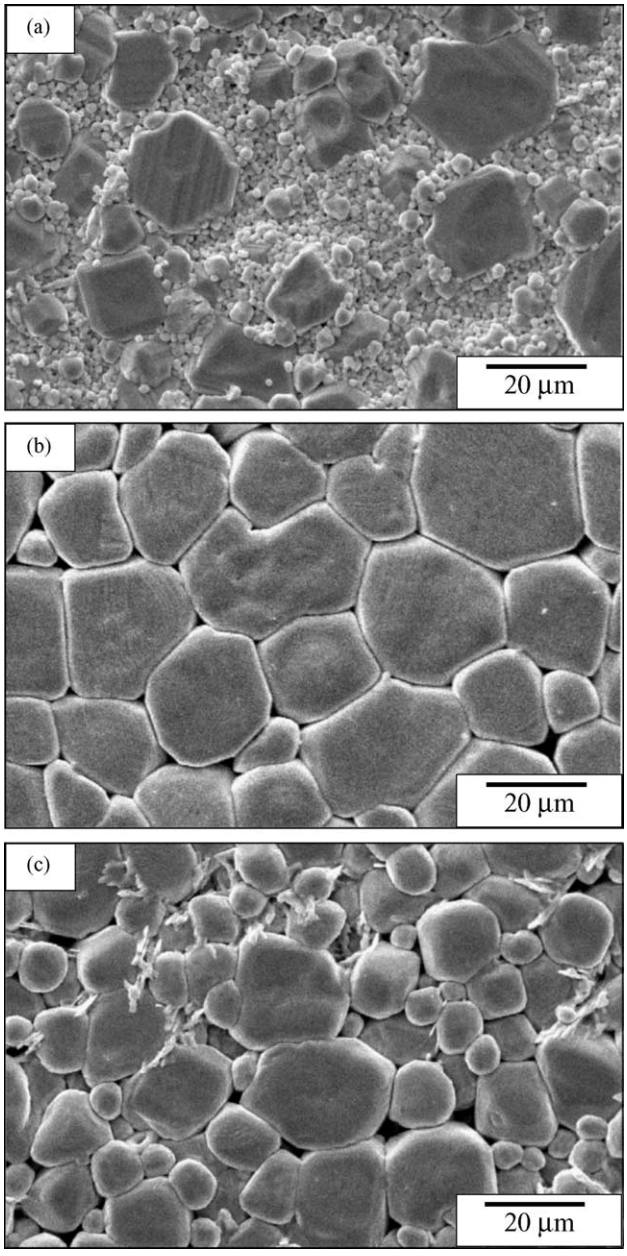

Fig. 4. SEM micrographs of as-sintered surfaces of: (a) Sb-BST + TiO_2 (composition 2) sintered at 1350 °C; (b) Sb-BST + TiO_2 (composition 2) sintered at 1400 °C; (c) Sb-BST + TiO_2/SiO_2 (composition 3) sintered at 1350 °C.

Fig. 3), leading to a dissolution–re-precipitation mass transport mechanism.[27] In comparison to the other two samples, the microstructures of composition 3 were more porous, the grain size distributions were not bimodal, and the maximum grain sizes were smaller (∼25 μm), Fig. 4(c); there was little change in grain size with increased sintering temperatures.

Backscattered SEM imaging, along with X-ray mapping, were performed on polished sections of the sintered ceramics to investigate compositional differences within the microstructures. For both compositions 1 and 2, an intergranular phase was evident which was richer in Ti than the Sb-BST

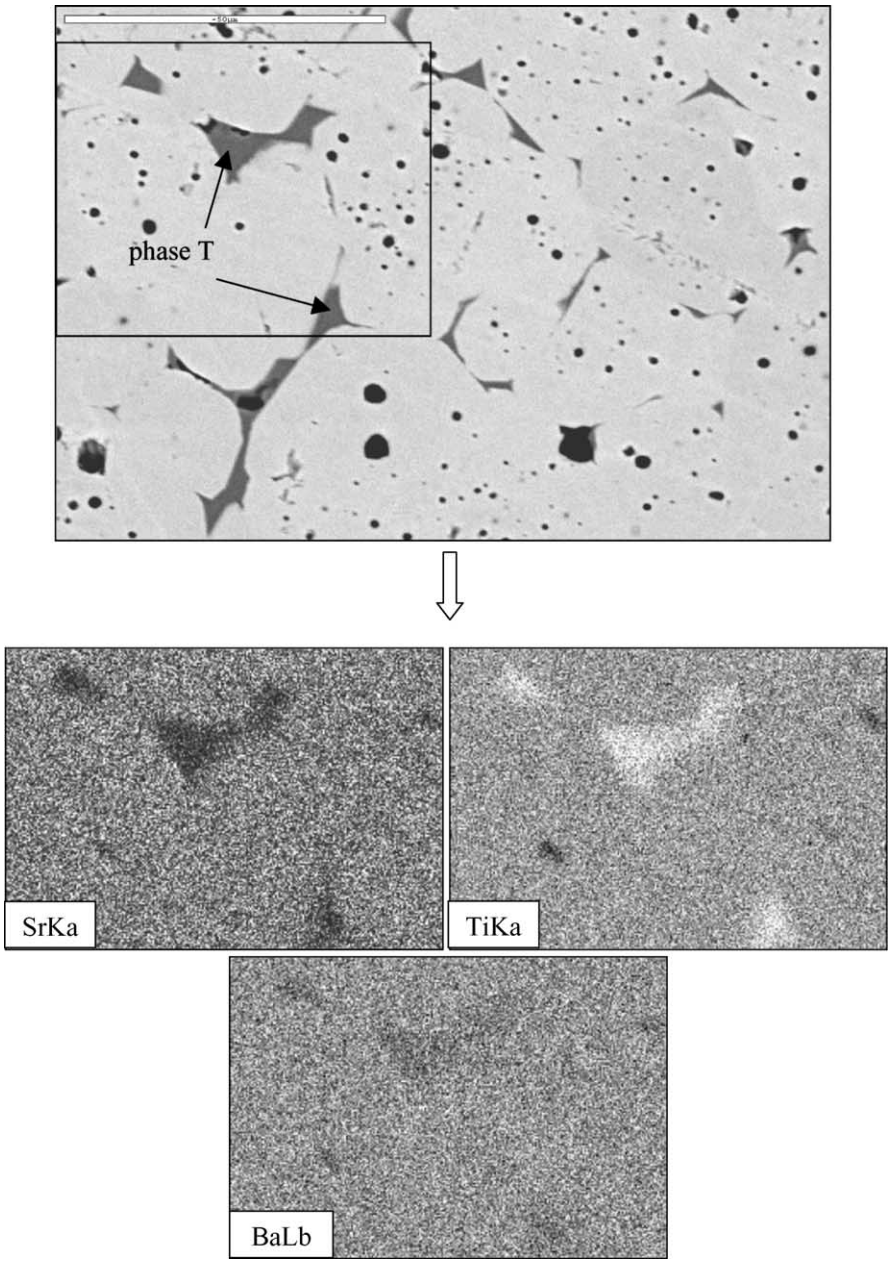

Fig. 5. Backscattered electron image (BEI) and X-ray maps of a polished sample of Sb-BST (composition 1) sintered at 1400 °C for 1 h.

matrix grains, and contained much less Sr, Figs. 5 and 6. This phase is referred to as phase T. In composition 3, phase T was again present but an additional phase, labelled S, was also observed, Fig. 7. Phase S was Si-rich, and with similar Ba levels, but lower Ti and Sr levels to the matrix Sb-BST grains. These qualitative descriptions are in agreement with the relative elemental contents of BST and the 6:17 and 2:1:2 secondary phases identified by XRD. Hence phase T was assumed to be the phase identified as 6:17 by XRD and phase S the 2:1:2 phase.

TEM-EDX and TEM-electron diffraction were used to provide more detailed information on the two intergranular phases in composition 3. The EDX results (semi-quantitative), showed only Ba, Sr and Ti in the matrix; the low level of added Sb was not detected, Fig. 8. Peak overlap made it difficult to determine any differences in Ba/Ti ratios in the EDX spectra from the matrix and from phase T. However, it did provide an indication of Sr in phase T, Fig. 8. Therefore, phase T, which XRD data had suggested to be $Ba_6Ti_{17}O_{40}$, was more probably a Sr-substituted phase, $(Ba,Sr)_6Ti_{17}O_{40}$. The other secondary phase analysed by EDX contained Ba, Ti and Si with low levels of Sr, Fig. 8. Therefore, this phase was the Si-containing phase S, suggested by XRD to be $Ba_2TiSi_2O_8$. TEM-EDX, as with phase T, indicated a low level of Sr substitution. An electron probe microanalysis (EPMA) study has confirmed that phase T was

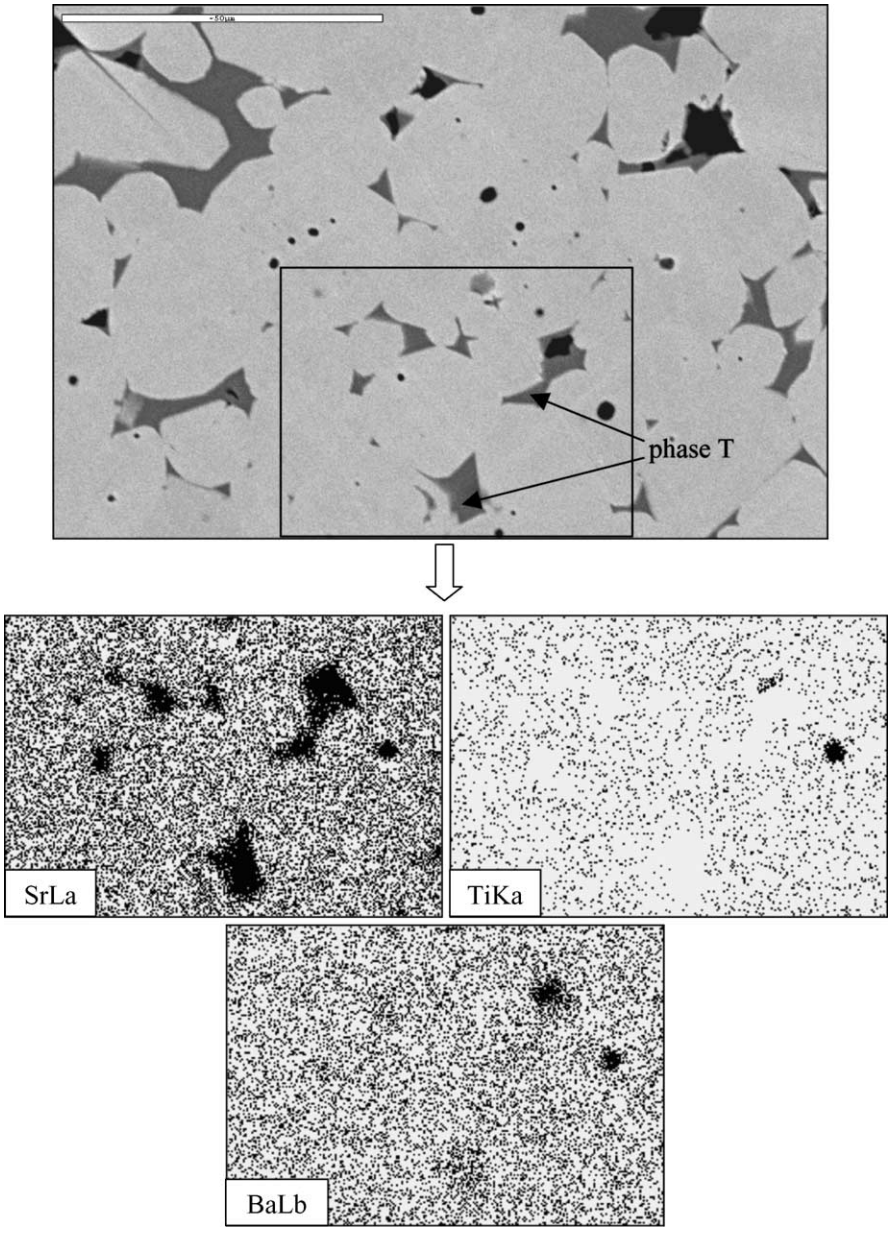

Fig. 6. BEI and X-ray maps of a polished sample of Sb-BST + TiO_2 (composition 2) sintered at 1400 °C for 1 h.

the 6:17 phase; analysis data implied a degree of beam overlap with the matrix phase, nevertheless the data was consistent with the composition being $(Ba_{1-x}Sr_x)_6Ti_{17}O_{40}$ with $x \sim 0.01$. The EPMA data for phase S revealed that the Si to Ti ratio deviated from that of fresnoite ($Ba_2TiSi_2O_8$) giving an actual formula of: $Ba_{1.95}Sr_{0.05}Ti_{1.2}Si_{1.8}O_8$. This is close to the limiting composition reported for substitution of Ti^{4+} on Si^{4+} sites in fresnoite.[28] The full results of the EPMA study, will be reported in a later publication.

Electron diffraction patterns provided confirmation that the phases being analysed by SEM-BEI and TEM-EDX were the same phases giving rise to the additional XRD peaks in Fig. 2. Examples of bright field and dark field images, together with corresponding selected area electron diffraction (SAED) patterns are shown in Fig. 9, for phase T, and in Fig. 10 for phase S. The SAED patterns could be indexed on the basis of the published XRD powder data for the $Ba_6Ti_{17}O_{40}$,[24] and $Ba_2TiSi_2O_8$,[25] parent, non-Sr-substituted phases. For monoclinic $Ba_6Ti_{17}O_{40}$ the reported lattice parameters a, b and c are 9.887 Å, 17.097 Å, and 18.918 Å, respectively, with $\beta = 98.72°$; values of a, b and c estimated from the indexed TEM-SAED patterns (assuming $\beta = 98.72°$) for the Sr-substituted phase T, were 9.88 Å, 17.52 Å and 18.86 Å. For tetragonal $Ba_2TiSi_2O_8$ the reported lattice parameters, a and c are 8.542 Å and 5.219 Å, respectively; values of a and c estimated from measurements of the TEM-SAED patterns of Sr-substituted phase S were 8.58 Å and 5.18 Å. TEM images, Fig. 10, indicated that the liquid formed

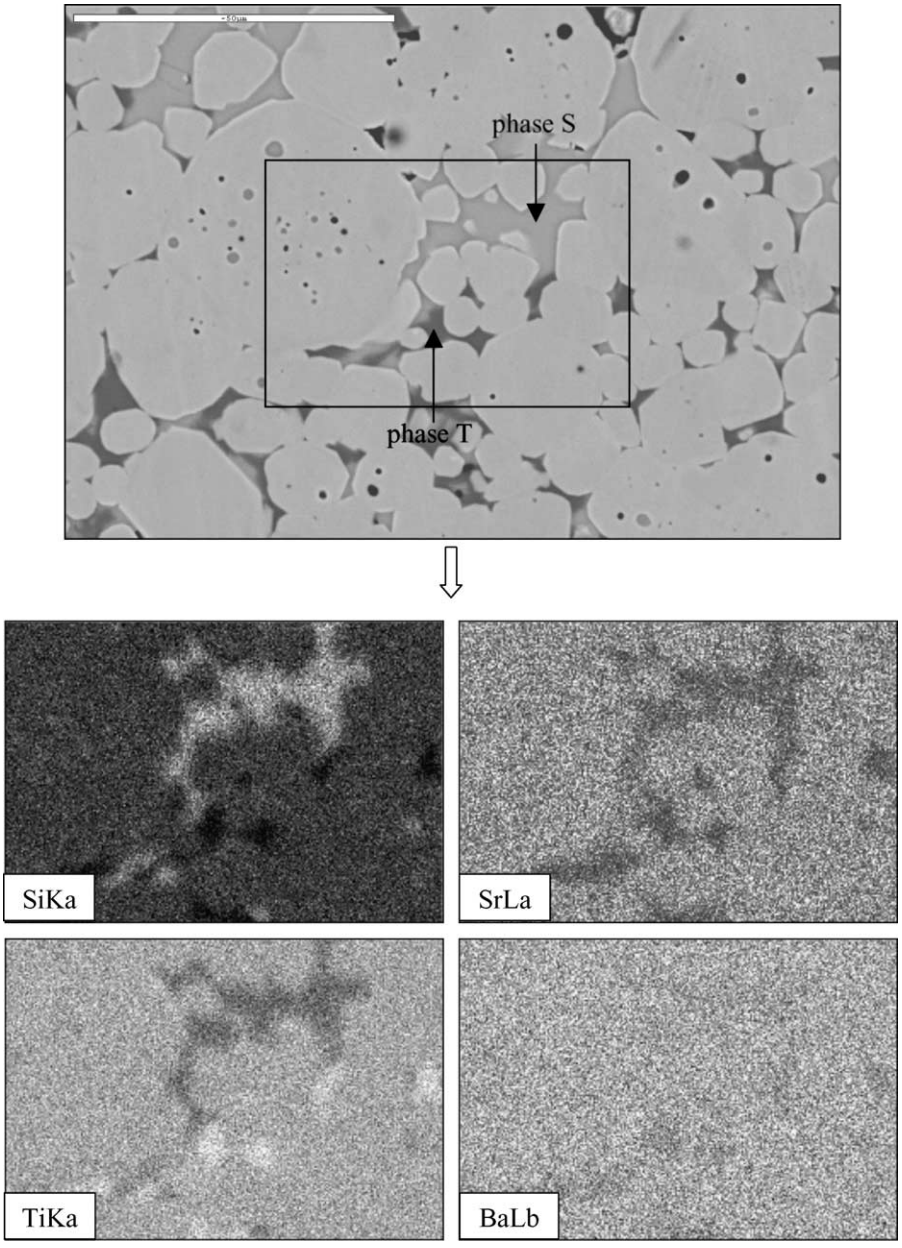

Fig. 7. BEI and X-ray maps of a polished sample of Sb-BST + TiO_2/SiO_2 (composition 3) sintered at 1400 °C for 1 h.

at high temperatures had wet at least some of the grains, and flowed along grain boundaries. It is possible that some dewetting occurred on cooling, resulting in segregation to triple points and other intergranular regions resulting in pockets of second phase, as illustrated in Fig. 7.

All of the samples exhibited PTCR behaviour, but there were variations dependent on sintering temperatures and additives. The resistivity–temperature (ρ–T) characteristics of samples of each of the three compositions, sintered at 1450 °C are plotted in Fig. 11 and results, for all samples are summarised in Table 1. The measurements were carried out using a silicone oil bath to heat the samples; this limited the upper temperatures to around 300 °C. For compositions 1 and 2, increasing the sintering temperature decreased the room temperature resistivity, ρ_{RT}, from >30 Ω cm for 1350 °C, to values of ∼10 Ω cm and 14 Ω cm for Sb-BST and Sb-BST + TiO_2, respectively, Table 1. There was no significant variation in ρ_{RT} with sintering temperature in the case of the SiO_2 + TiO_2 additive, all samples giving a value of 8–14 Ω cm. The SiO_2+TiO_2 additive enhanced the PTCR effect, by producing higher values of maximum resistivity (ρ_{max}), for samples fabricated at higher sintering temperatures, Table 1. The steepest rise in resistivity occurred for a sintering temperature of 1450 °C, giving a ρ_{max} value of 1.2×10^5 Ω cm, compared to $<2.5 \times 10^4$ Ω cm for the other two compositions, Table 1. This represents a resistance increase (ρ_{max}/ρ_{RT}) of $\sim 10^4$ be-

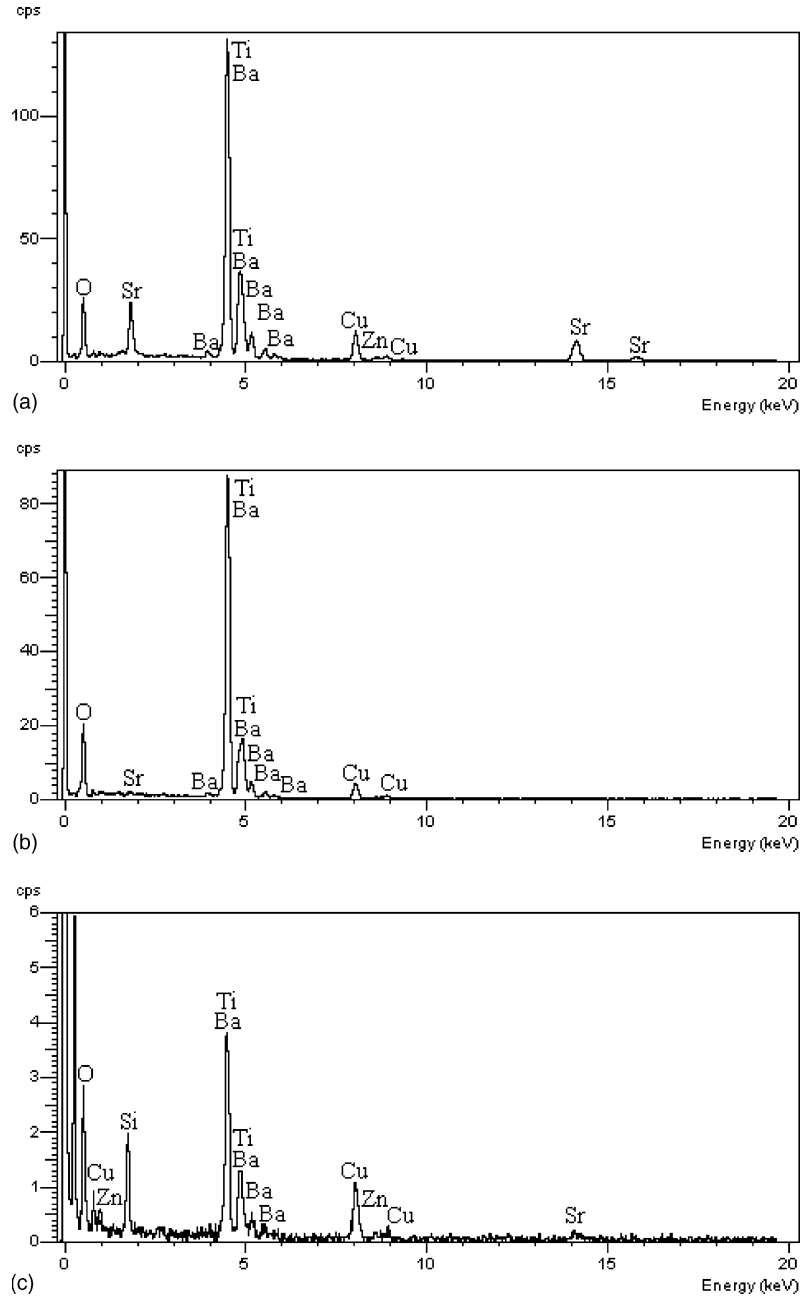

Fig. 8. TEM-EDX data for Sb-BST + TiO_2/SiO_2 (composition 3): (a) matrix grain; (b) intergranular phase T (6:17); (c) intergranular phase S (2:1:2).

Table 1
Summary of values of: room temperature resistivity, ρ_{RT}; the ratio ρ_{max}/ρ_{RT} (ρ_{max} = maximum resistivity on raising the temperature); T_{max}, the temperature corresponding to ρ_{max} as a function of sintering temperature and composition

Sintering temperature (^oC)	Samples								
	Sb-BST			Sb-BST+TiO_2			Sb-BST + TiO_2/SiO_2		
	ρ_{RT} (Ω cm)	ρ_{max}/ρ_{RT}	T_{max} ($^\circ$C)	ρ_{RT} (Ω m)	ρ_{max}/ρ_{RT}	T_{max} ($^\circ$C)	ρ_{RT} (Ω cm)	ρ_{max}/ρ_{RT}	T_{max} ($^\circ$C)
1275	–	–	–	–	–	–	13	5.0×10^2	265
1300	–	–	–	–	–	–	8	1.8×10^3	260
1350	35	7.5×10^1	260	38	9.2×10^2	250	11	2.6×10^3	275
1400	11	1.9×10^3	270	18	1.7×10^3	275	12	4.6×10^3	280
1450	10	2.2×10^3	270	14	1.7×10^3	280	14	9.0×10^3	280

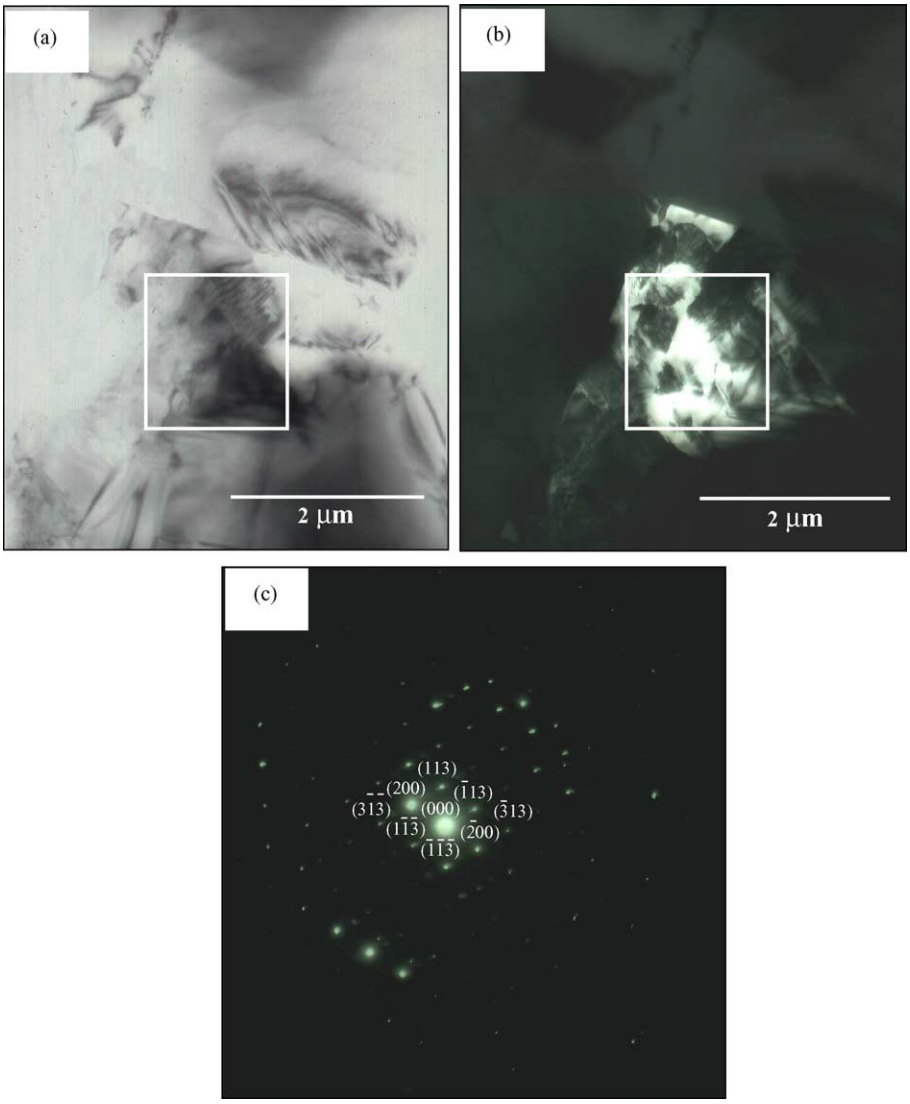

Fig. 9. TEM data for phase T present in the Sb-BST + TiO_2/SiO_2 specimen (composition 3): (a) bright field image; (b) dark field image (200 reflection); (c) corresponding electron diffraction pattern that has been indexed to the $[0\,\bar{3}\,1]$ crystal axis of phase T lying parallel to the electron beam from the area indicated in (a) and (b). The ED pattern is indexed using XRD powder data for $Ba_6Ti_{17}O_{40}$.[24]

tween room temperature and 280 °C for the SiO_2 + TiO_2 additive. In an additional experiment, PTCR data were obtained for a Sb-BST + TiO_2/SiO_2 sample with 0.02 mol% of added manganese oxide, Fig. 11(b); there was a substantial increase in resistivity, with the value of ρ_{RT} increasing to ~5 × 10^2 Ω cm and the ρ_{max}/ρ_{RT} ratio increasing to ~$10^{5.8}$ (for a sample sintered at 1350 °C).

4. Discussion

For the more extensively studied $BaTiO_3$ system, 1–4 mol% of excess TiO_2 is often used to promote a liquid phase during sintering, and so aid densification. The BaO–TiO_2 phase diagram indicates that at equilibrium, a small excess of TiO_2 added to $BaTiO_3$ results in a liquid being formed at a temperature of ~1330 °C, with a mixture of $BaTiO_3$ and $Ba_6Ti_{17}O_{40}$ solid phases co-existing at equilibrium below this temperature.[10] From the present study into Sb-BST with an added nominal 1 mol% TiO_2 (composition 2), there was no evidence of enhanced densification (Fig. 3). Phase equilibria for the ternary BaO–SrO–TiO_2 system, published for an isothermal section at 1250 °C and 1400 °C provides an explanation for this and for the phases produced during sintering.[29,30] The earlier version of the diagram at 1400 °C[29] is broadly similar to the 1250 °C diagram,[30] reproduced in Fig. 12, but with $(Ba,Sr)Ti_3O_7$ being reported in place of $(Ba,Sr)_6Ti_{17}O_{40}$.

From the phase diagrams, for an overall composition of $(Ba_{0.8}Sr_{0.2})TiO_3$ plus 1 mol% of TiO_2, a two-phase field of $(Ba,Sr)TiO_3$ and $(Ba,Sr)_6Ti_{17}O_{40}$ coexisting solid solutions is indicated at temperatures of 1250–1450 °C.[29,30] Notwithstanding any significant effects due to the 0.15 mol% of added Sb_2O_3, composition 2 would be expected from the phase dia-

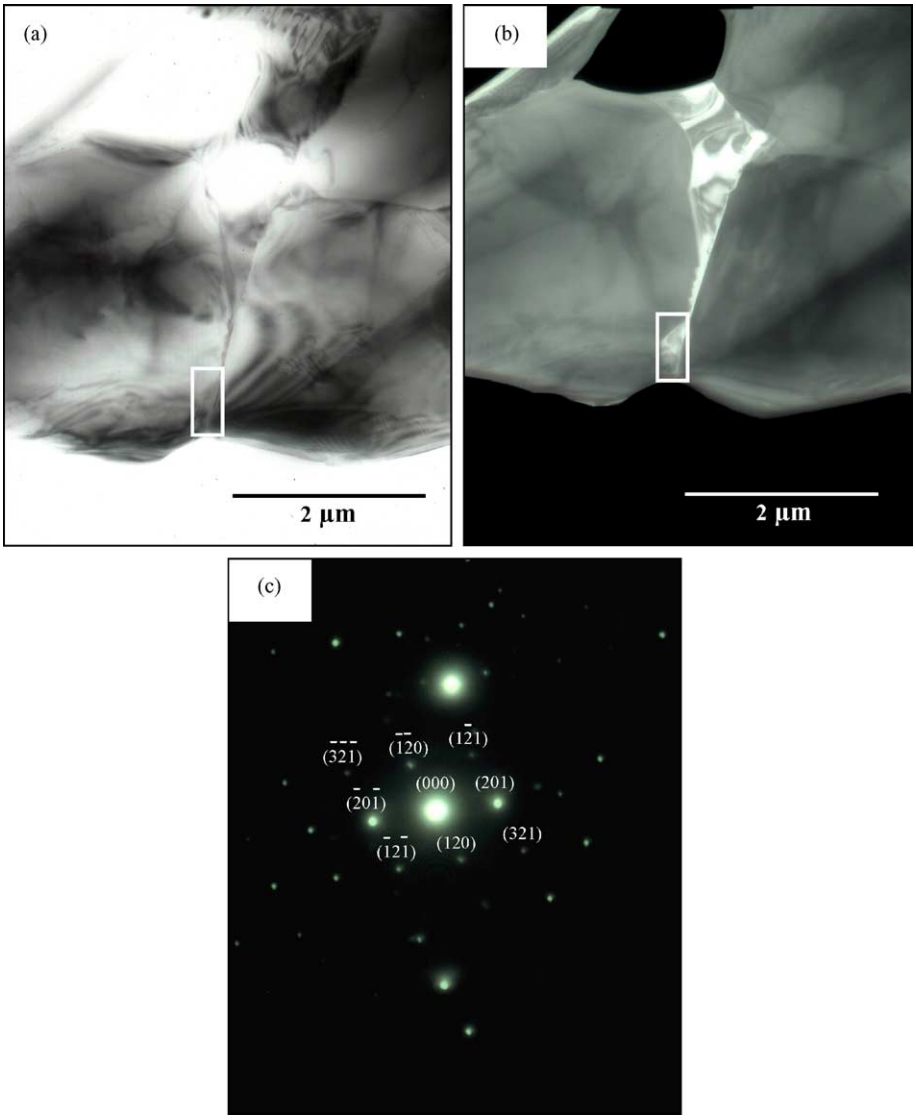

Fig. 10. TEM data for Phase S for Sb-BST + TiO_2/SiO_2 (composition 3): (a) bright field image; (b) dark field image (2 0 1 reflection); (c) corresponding electron diffraction pattern that has been indexed to the [2̄14] crystal axis parallel to the electron beam from the area indicated in (a) and (b). The ED pattern is indexed using XRD powder data for $Ba_2TiSi_2O_8$.[25]

gram to be a mixture of ∼98 mol% (Ba,Sr)TiO_3 and ∼2mol% (Ba,Sr)$_6Ti_{17}O_{40}$ solid solution phases, with no liquid present. The maximum compositional extent of Sr substitution in 'B_6T_{17}ss' ((Ba,Sr)$_6Ti_{17}O_{40}$) is shown by the phase diagram to be around 2 mol%, Fig. 12. The experimental phase and compositional analysis results are therefore consistent with the predictions from the equilibrium phase diagrams. The phase diagrams also explain why, in contrast to the situation for $BaTiO_3$, adding excess TiO_2 to BST produces no reduction in sintering temperature. In the BST-TiO_2 system no liquid is formed (at equilibrium) at temperatures up to 1400 °C. However, added TiO_2 did produce a microstructural effect, bringing about a reduction in grain size; this may have been due to grain pinning effects associated with the second phase (Ba,Sr)$_6Ti_{17}O_{40}$particles. (The unmodified composition, Sb-BST, also contained (Ba,Sr)$_6Ti_{17}O_{40}$ but at much lower levels, and therefore the microstructural effect would be much greater in Sb-BST + TiO_2.)

There are several possible reasons why lower levels of the Ti-rich second phase, (Ba,Sr)$_6Ti_{17}O_{40}$, may have been present in sintered samples of unmodified Sb-BST. The (Ba,Sr)$_6Ti_{17}O_{40}$ could be present simply due to inadequate mixing of the components in the starting powders, giving TiO_2 rich regions which produce (Ba,Sr)$_6Ti_{17}O_{40}$ at sintering temperatures. Alternatively it could signify a solid solution mechanism involving Ti^{4+} vacancy formation as charge compensation for Sb^{3+} substitution on divalent A sites. It is reported that at low dopant concentrations, the Sb^{3+} ions occupy the Ba^{2+} sites, and at higher dopant concentrations, they can occupy the Ba^{2+} sites and/or Ti^{4+} sites.[31–33] However, based on careful phase diagram studies, coupled to results of impedance spectroscopy, a Ti vacancy mecha-

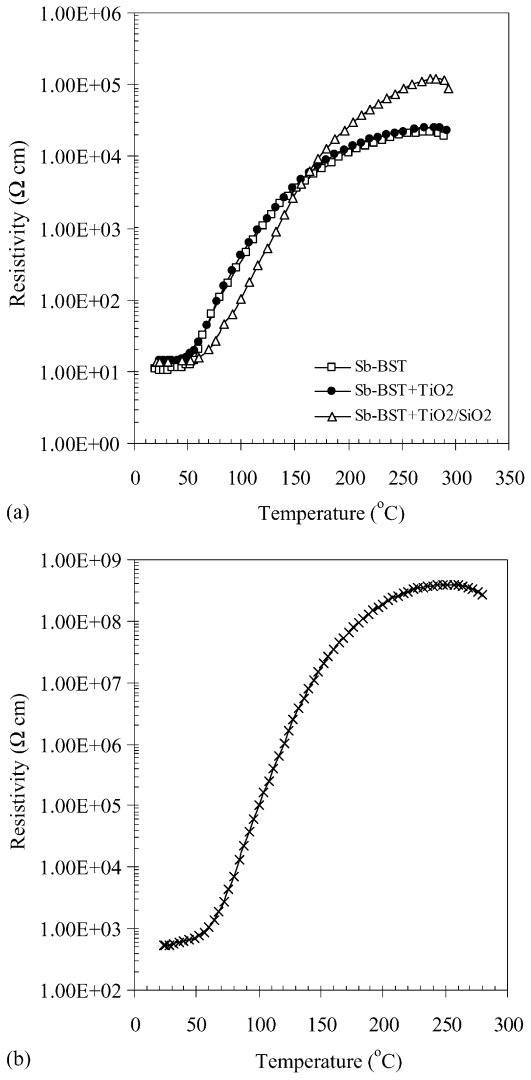

Fig. 11. The resistivity–temperature characteristics of the three compositions sintered at 1450 °C, together with data showing an enhanced PTCR response for TiO_2/SiO_2 + 0.02 mol% manganese oxide sintered at 1350 °C.

nism has been suggested for a range of donor-doped PTCR compositions.[6,7,34] Because there was no compensating reduction in the TiO_2 content of the starting powders used here, solid solution mechanisms involving Ti vacancy formation, would naturally generate 'excess' TiO_2 during calcination and/or sintering. For example, if the solid solution formation mechanism involved Ti vacancy creation to compensate for the additional charge of Sb^{3+} on a Ba^{2+} (or Sr^{2+}) site, giving a formula, $(Ba,Sr)_{1-x}Sb_xTi_{1-x/4}O_3$, then our starting mixture of 0.15 mol% Sb_2O_3 ($x = 0.003$), with no compensating reduction in the TiO_2 content, would result in an 'excess' of TiO_2 being released, equivalent to $x = 0.003/4$, or 0.075 mol% excess TiO_2. More speculatively, a complex mechanism involving some Sb^{5+} formation and substitution on Ti^{4+} sites may occur, again giving excess TiO_2 (for Sb_2O_5 doping, the Sb^{5+} ions are reported to occupy the Ti^{4+} sites[33]).

Because of this liberated TiO_2 the starting composition of Sb-BST (composition 1) would therefore lie in the same two-phase field in the equilibrium phase diagram as BST + TiO_2 (composition 2), but would give a much lower proportion of $(Ba,Sr)_6Ti_{17}O_{40}$ (according to lever rule calculations). By a similar argument, compositions 2 and 3, namely Sb-BST + TiO_2 and Sb-BST + (TiO_2/SiO_2) would therefore contain a total excess of ~1.1 mol% TiO_2.

For composition 3, with co-additions of SiO_2 and TiO_2 we have been unable to find relevant quaternary phase diagram information. A published phase diagram for the join, $BaTiO_3$–SiO_2 indicates a solidus temperature of ~1260 °C for additions of up to 28% of silica (although there is debate about aspects of this version of the diagram and the system has been shown not to be a true binary).[35,36] Our experimental results for composition 3 showed that there was a major increase in density on moving from a sintering temperature of 1200 °C to 1250 °C. This suggests liquid formation and a solidus temperature between 1200 °C and 1250 °C, for Sb-BST + TiO_2/SiO_2.

The XRD and TEM-ED results for Sb-BST + (TiO_2/SiO_2) indicated that $(Ba,Sr)_2TiSi_2O_8$ (fresnoite) was the main phase which crystallises from the liquid during cooling; this co-existed with a small amount of $(Ba,Sr)_6Ti_{17}O_{40}$. EPMA results indicated substitution of Ti^{4+} for Si^{4+} on the tetrahedral sites of fresnoite giving a formula: $Ba_{1-y}Sr_yTi_{1+x}Si_{2-x}O_8$. Other workers studying the system, $Ba_2Ti_{1+x}Si_{2-x}O_8$, $0 \leq x \leq 0.14$[28] have reported that variation in the Si/Ti ratio, results in essentially identical XRD patterns, which explains why our XRD and TEM–SAED data showed close agreement with standard data for $Ba_2TiSi_2O_8$. The level of Sb substitution (if any) in the intergranular phases is uncertain.

The 'parent' $BaTiO_3$ composition, co-modified with small amounts of TiO_2 and SiO_2, has been reported to produce a glassy grain boundary phase crystallising to $BaTiSiO_5$.[26] However, the existence of $BaTiSiO_5$ has been questioned and we found no evidence of it. More commonly silica additions are reported to give a mixture of $BaTiO_3$, $Ba_2TiSi_2O_8$ (fresnoite) and $Ba_6Ti_{17}O_{40}$.[37,38] Whereas we have demonstrated that BST + TiO_2 produced a very different phase mixture to $BaTiO_3$–TiO_2; the present results for BST demonstrate that there are close similarities in the phases produced for SiO_2 additions to BST, and reported results for $BaTiO_3$.

Other workers studying exaggerated grain growth in $BaTiO_3$ with added SiO_2 have also reported fresnoite.[35,39,40] It has been suggested that secondary or exaggerated grain growth in $BaTiO_3$–SiO_2 is due to the formation of the intergranular silica-rich liquid at temperatures between 1260 °C and 1320 °C.[26] However, the present results demonstrate an absence of exaggerated grain growth in Sb-BST + (TiO_2/SiO_2) samples, despite the evidence that a silica-rich liquid formed during sintering.

There are reports that $Ba_6Ti_{17}O_{40}$ particles in $BaTiO_3$, present as consequence of added TiO_2, are the origin of exaggerated grain growth, resulting in the formation of elongated {1 1 1} twinned $BaTiO_3$ grains. The secondary,

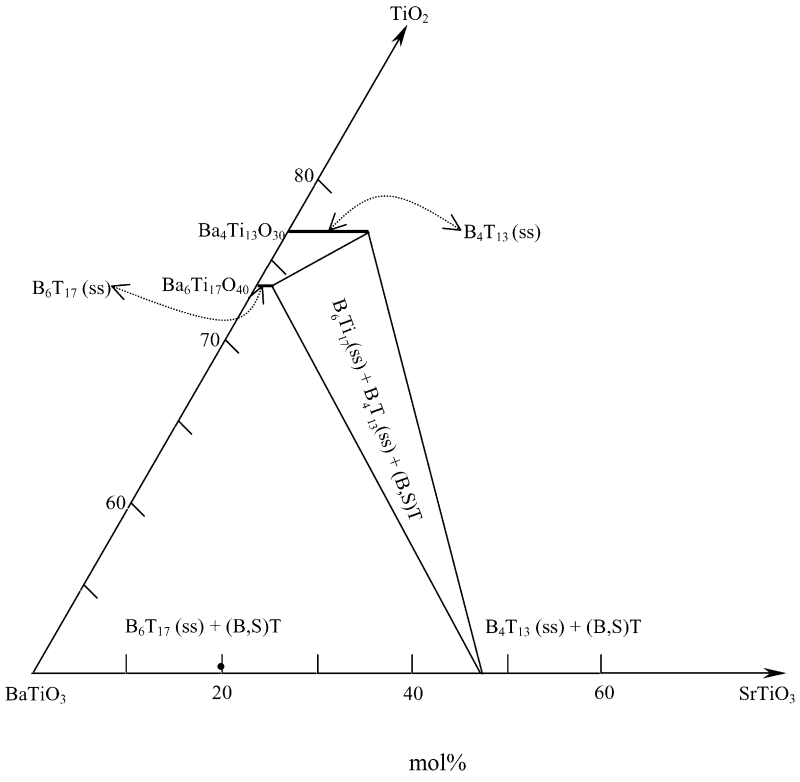

Fig. 12. Phase equilibria for part of the BaO–SrO–TiO_2 system at 1250 °C[30] which is broadly similar to published data for 1400 °C[29] ((●) composition in this present work, for Sb-BST + 1 mol% TiO_2). B_6T_{17} (ss) = Sr-substituted $Ba_6Ti_{17}O_{40}$; B_4T_{13} (ss) = Sr-substituted $Ba_4Ti_{13}O_{30}$.

elongated {1 1 1} twinned grains were said to form by nucleation from the $Ba_6Ti_{17}O_{40}$ particles.[30] In our Sb-BST and Sb-BST + TiO_2 samples, which each contained (Ba,Sr)Ti_6O_{17} and exhibited exaggerated grain growth, we did not observe any of the characteristic, elongated grains reported to be {1 1 1} twins in $BaTiO_3$, and also reported in BST prepared by other research groups.[30,41–43] The reasons for this discrepancy are unclear.

Each of the three compositions produced different PTCR responses. For a given composition, the effects of sintering temperature are likely to be related to microstructural changes and to changes in the distributions of dopants and defects at grain boundary regions. For all compositions, the most favourable PTCR responses were obtained in ceramics fabricated at the highest sintering temperatures. Possibly this was because of improved mass transport at the highest temperatures, producing improved grain boundary structures and well defined barrier layers.

Overall the best PTCR response of the three compositions was in the sample of Sb-BST co-modified with TiO_2 and SiO_2 (composition 3), sintered at 1450 °C. The microstructure of ceramics with this composition were very different to the other compositions, being more porous, which would be expected to promote oxygen diffusion to the grain boundaries, and increases the resistivity of the grain–grain boundary interfaces.[6,7] The smaller average grain size, and greater grain boundary surface area may also contribute to different PTCR characteristics for the TiO_2 + SiO_2 additive composition. As mentioned in the introduction, AST is often added to $BaTiO_3$ and BST ceramics to promote liquid phase sintering. Cheng et al.[15] have added varying amounts of AST to Sb-BST, which allows a direct comparison with results obtained here for 1 mol% TiO_2 + 3 mol% SiO_2.[1]

The room temperature resistivities, ρ_{RT}, for Sb-BST + AST were reportedly higher, of the order 10^2–10^3 Ω cm, depending on total additive content, compared to 8–14 Ω cm here for TiO_2 + SiO_2. The maximum resistivities on heating to higher temperatures, ρ_{max}, were also higher for the AST system, giving a ρ_{max}/ρ_{RT} ratios as high as $10^{5.6}$ compared to $\sim 10^4$ for the more simple TiO_2 + SiO_2 additives in this work. The 1 mol% TiO_2 + 3 mol% SiO_2 additive composition was selected for detailed study after it had been found to give the most favourable properties in preliminary trials of different amounts of additive, and different TiO_2/SiO_2 ratios.[44] Lai et al.[45] suggested that AST enhanced the PTCR effect (in Nd-doped BST) by increasing acceptor state density (electron traps) at grain boundaries. More recently Lee et al.[14] illustrated the importance of an acceptor-rich BST surface layer precipitated from an AST liquid which was assumed to be rich in acceptor impurities; Al^{3+} is a well-known acceptor in perovskites,[2,46] substituting for Ti^{+4}. Therefore,

[1] 1 mol AST = 0.255 mol Al_2O_3 + 0.562 mol SiO_2 + 0.187 mol TiO_2; 1 mol of the 'ST' used here = 0.25mol TiO_2 + 0.75 mol SiO_2.

the lower resistivities of Sb-BST + TiO_2/SiO_2 obtained in the present study (with no added acceptors) indirectly supports the premise that Al^{3+} contained in AST plays a critical role as a compensating acceptor dopant, possibly being distributed along grain boundaries whilst the additive is in the liquid phase, reacting with BST surface layers and increasing their resistivity. By adding 0.02 mol% manganese oxide to the starting Sb-BST + TiO_2/SiO_2 mixture we found that ρ_{RT} could be increased to 530 Ω cm, and a ratio ρ_{max}/ρ_{RT} of $\sim 10^{5.8}$ was obtained, which is comparable to values reported for the AST sintering additive.

Another factor to consider when comparing the PTCR properties of the two liquid forming systems is the relative ease of oxygen diffusion through the liquid and along grain boundaries as the samples is cooled from sintering temperatures. West et al. have demonstrated the importance of oxygen non-stoichiometry in PTCR materials.[6,7,34] The electrical properties of the respective crystalline silicate grain boundary phases would also be important, but little is known as to how this factor influences the conduction barriers at grain interfaces.

In summary, although the benefits of adding sintering aids to PTCR ceramics have been demonstrated here and elsewhere, and acceptor species present in the liquid which is formed at the sintering temperatures may play an important role, the mechanisms leading to improvements in the PTCR response remain uncertain. Further studies utilising high resolution TEM and impedance spectroscopy to investigate the structure and conductivity of grain boundary regions for a range of additive compositions are likely to be of value.

5. Conclusions

A combined additive consisting of 3 mol% SiO_2 and 1 mol% TiO_2 was effective in reducing the sintering temperatures of Sb-doped BST ceramics by inducing liquid phase sintering. The microstructures were more porous than those of Sb-BST, or those with only TiO_2 as an additive.

The combined additive, on cooling, resulted in intergranular regions containing crystalline phases of a fresnoite solid solution $Ba_{1.95}Sr_{0.05}Ti_{1.2}Si_{1.8}O_8$ and $(Ba,Sr)_6Ti_{17}O_{40}$ (with ~1 mol% Sr^{2+} for Ba^{2+} substitution). There was TEM evidence that the liquid phase wet the boundaries between individual grains at high temperatures, but there were many large pockets of secondary phases in the microstructures.

As well as reducing sintering temperatures, the SiO_2 + TiO_2 additive enhanced the PTCR effect: room temperature resistivities were <14 Ω cm and in terms of the PTCR effect, maximum values of resistivity were around five times higher than for the other compositions. The ratio ρ_{max}/ρ_{RT} increased with increasing sintering temperatures, reaching a maximum value of $\sim 10^4$. This improvement in PTCR properties may have been due to greater oxidation of grain boundary layers during processing as a result of the more porous microstructure. Additions of manganese oxide to the Sb-BST–SiO_2 + TiO_2 system raised the value of ρ_{max}/ρ_{RT} to $\sim 10^{5.8}$.

For samples of Sb-BST + TiO_2, the absence of any evidence of liquid phase sintering with respect to densification experiments, and the presence of a $(Ba,Sr)_6Ti_{17}O_{40}$ intergranular phase was consistent with published phase equilibria for the $BaTiO_3$–$SrTiO_3$–TiO_2 system. However, the additive did have a role in influencing microstructures by reducing grain growth. The presence of smaller amounts of the same $(Ba,Sr)_6Ti_{17}O_{40}$ phase in samples with no nominal starting excess of TiO_2 may have been indicative of a solid solution mechanism involving charge compensation by the formation of Ti^{4+} vacancies, as the starting powders were prepared without any compensating reduction in TiO_2 content.

Acknowledgements

The authors wish to thank Tim Comyn, Steve McBride, P. Vogel and other colleagues for advice and practical support. Thanks are expressed to Eric Condliffe for EPMA and data interpretation. P. Bomlai wishes to thank the Royal Thai Government and Graduate school, Chiang Mai University for a scholarship.

References

1. He, Z., Ma, J., Qu, Y. and Feng, X., Effect of additives on the electrical properties of a $(Ba_{0.92}Sr_{0.08})TiO_3$-based positive temperature coefficient resistor. *J. Eur. Ceram. Soc.*, 2002, **22**, 2143.
2. Cheng, H. F., Effect of sintering aids on the electrical properties of positive temperature coefficient of resistivity $BaTiO_3$ ceramics. *J. Appl. Phys.*, 1989, **66**, 1382–1387.
3. Kim, J. G., Synthesis of porous (ba,Sr)TiO_3 ceramics and PTCR characteristics. *Mats. Chem. Phys.*, 2002, **78**, 154–159.
4. Hewang, W., Resistivity anomaly in doped barium titanate. *J. Am. Ceram. Soc.*, 1964, **47**, 484–490.
5. Jonker, G. H., Some aspect of semiconducting barium titanate. *Solid State Electron.*, 1964, **8**, 895–903.
6. Morrison, F. D., Sinclair, D. C. and West, A. R., An alternative explanation for the origin of the resistivity anomaly in La-doped $baTiO_3$. *J. Am. Ceram. Soc.*, 2001, **84**, 474–476.
7. Morrison, F. D., Sinclair, D. C. and West, A. R., Doping mechanisms and electrical properties of La-doped $BaTiO_3$. *Int. J. Inorg. Mater.*, 2001, **3**, 1205–1210.
8. Zhao, J., Li, L. and Gui, Z., Influence of lithium modification on the properties of Y-doped $Sr_{0.5}Pb_{0.5}TiO_3$ thermistors. *Sens. Actuat. A*, 2001, **95**, 46–50.
9. Kim, J-G., Cho, W-S. and Park, K., Effect of atmophere on the PTCR characteristics of porous (ba,Sr)TiO_3 ceramics. *Mater. Sci. Eng. B*, 2001, **83**, 123–129.
10. Kirby, K. W. and Wechsler, B. A., Phase relations in the barium titanate-titanium oxide system. *J. Am. Ceram. Soc.*, 1991, **84**, 1841–1847.
11. Al-Allak, H. M., Parry, T. V., Russell, G. J. and Woods, J., Effects of aluminium on the electrical and mechanical properties of PTCR $BaTiO_3$ ceramics as a function of the sintering temperature. *J. Mater. Sci.*, 1988, **23**, 1083–1089.
12. Rase, D. E. and Roy, R., Phase equilibria in the system $BaTiO_3$–SiO_2. *J. Am. Ceram. Soc.*, 1955, **38**, 389–395.

13. Matsuo, Y., Fujimura, M., Sasahi, H., Nagase, K. and Hayakawa, S., Semiconducting $BaTiO_3$ with Al_2O_3 SiO_2 and TiO_2. *Am. Ceram. Soc. Bull.*, 1968, **47**, 292–297.
14. Lee, J. K., Park, J. S., Hong, K. S., Ko, K. H. and Lee, B. C., Role of liquid phase in PTCR characteristics of $(Ba_{0.7}Sr_{0.3})TiO_3$ ceramics. *J. Am. Ceram. Soc.*, 2002, **85**, 1173–1179.
15. Cheng, H. F., Lin, T. F., Hu, C. T. and Lin, I. N., Effect of sintering aids on microstructure and PTCR characteristics of $(Sr_{0.2}Ba_{0.8})TiO_3$ ceramics. *J. Am. Ceram. Soc.*, 1993, **76**, 827–832.
16. Chen, C.-S., Cheng, H.-F. and Lin., I.-N., Positive temperature coefficient properties of $(Sr_{0.2}Ba_{0.8})TiO_3$ prepared by microwave sintering technique. *Ferroelectrics*, 2002, **270**, 21–26.
17. Joint Committee for Powder Diffraction standard, file No. 44-0093.
18. Joint Committee for Powder Diffraction standard, file No. 41-0373.
19. Joint Committee for Powder Diffraction standard, file No. 84-2213.
20. Joint Committee for Powder Diffraction standard, file No. 22-0510.
21. Joint Committee for Powder Diffraction standard, file No. 26-1402.
22. Joint Committee for Powder Diffraction standard, file No. 83-1459.
23. Cullity, B. D. and Stock, S. R., *Elements of X-ray Diffraction*. Prentice Hall, New Jersey, 2001.
24. Joint Committee for Powder Diffraction standard, card No. 77-1566.
25. Joint Committee for Powder Diffraction standard, card No. 84-0924.
26. Saldaňa, J. M., Mullier, B. and Schneider, G. A., Preparation of $BaTiO_3$ single crystals using the modified SiO_2-exaggerated grain growth method. *J. Eur. Ceram. Soc.*, 2002, **22**, 681–688.
27. Liu, G. and Roseman, R. D., Effect of BaO and SiO_2 addition on PTCR $BaTiO_3$ ceramics. *J. Mater. Sci.*, 1999, **34**, 4439–4445.
28. Coats, A. M., Hirose, N., Marr, J. and West, A. R., Tetrahedral Ti^{4+} in the solid solution $Ba_2Ti_{1+x}Si_{2-x}O_8$ ($0 \leq x \leq 0.14$). *J. Solid State Chem.*, 1996, **126**, 105–107.
29. Kwestroo, W. and Paping, H. A. M., The systems BaO–SrO–TiO_2, BaO–CaO–TiO_2, and SrO–CaO–TiO_2. *J. Am. Ceram. Soc.*, 1959, **42**, 292–299.
30. Lee, B.-K., Jung, Y.-I., Kang, S.-J. L. and Nowotny, J., $\{1\,1\,1\}$ Twin formation and abnormal grain growth in barium strontium titanate. *J. Am. Ceram. Soc.*, 2003, **86**, 155–160.
31. Sasaki, Y., Fujii, I., Matsui, T. and Morii, K., Influence of antimony doping on electrical properties of barium titanate ($BaTiO_3$) thin films. *Mater. Lett.*, 1996, **26**, 265–271.
32. Xue, L. A., Chen, Y. and Brook, R. J., The influence of ionic radii on the incorporation of trivalent dopants into $BaTiO_3$. *Mater. Sci. Eng. B.*, 1988, **1**, 193–201.
33. Brzozowski, E. and Castro, M. S., Influence of Nb^{5+} and Sb^{3+} dopants on the defect profile PTCR effect and GBBL characteristics of $BaTiO_3$ ceramics. *J. Eur. Ceram. Soc.*, 2004, **24**, 2499–2507.
34. Morrison, F. D., Sinclair, D. C. and West, A. R., Characterization of lanthanum-doped barium titanate ceramics using impedance spectroscopy. *J. Am. Ceram. Soc.*, 2001, **84**, 531–538.
35. Felgner, K. H., Müller, T., Langhammer, H. T. and Abicht, H.-P., Investigations on the liquid phase in barium titanate ceramics with silica additives. *J. Eur. Ceram. Soc.*, 2001, **21**, 1657–1660.
36. Robbins, C. R., Synthesis and growth of fresnoite ($Ba_2TiSi_2O_8$) from a TiO_2 flux and its relation to the system $BaTiO_3$–SiO_2. *J. Res. National Bureau Standard A. Phys. Chem.*, 1970, **74A**, 229–232.
37. Hesse, D., Graff, A., Senz, S. and Zakharov, N. D., Topotaxial reaction fronts in complex Ba–Ti–Si oxide systems studied by transmission electron microscopy. *Mater. Sci. Forum*, 1999, **294–296**, 597–600.
38. Abicht, H. P., Langhammer, H. T. and Felhner, K. H., The influence of silicon on microstructure and electrical properties of La-doped $baTiO_3$ ceramics. *J. Mater. Sci.*, 1991, **26**, 2337.
39. Belous, A. G., Makarova, S. J., Schacharov, O. A., Tschaly, W. P. and Gornikov, J. I., The system BaO–TiO_2-SiO_2 with varying ratios of the components. *Ukr. Chim. Zurn.*, 1987, **53**, 910–911.
40. Köppen, N. and Dietzel, A., About the system BaO–TiO_2-SiO_2. *Glastechn. Ber.*, 1976, **49**, 199–206.
41. Lee, B.-K. and Kang, S.-J. L., Necessary condition for the formation of $\{111\}$ twins in barium titanate. *J. Am. Ceram. Soc.*, 2000, **83**, 2858–2860.
42. Lee, B.-K. and Kang, S.-J. L., Second-phase assisted formation of $\{111\}$ twins in barium titanate. *Acta Mater.*, 2001, **49**, 1373–1373.
43. Lee, B.-K., Chung, S.-Y. and Kang, S.-J. L., Control of $\{1\,1\,1\}$ twin formation and abnormal grain growth in $BaTiO_3$. *Met. Mater.*, 2000, **6**, 301–304.
44. Bomlai, P., Sirikulrat, N. and Tunkasiri, T., Microstructures and positive temperature coefficient resistivity (PTCR) characteristics of high silicon addition barium-strontium titanate ceramics. *J. Mater. Sci.*, 2004, **39**, 1831–1835.
45. Lai, C. H., Weng, C. T. and Tseng, T. Y., The effects of Nd_2O_3 additives and Al_2O_3–SiO_2–TiO_2 sintering aids on the electrical resistivity of (Ba,Sr)TiO_3 PTCR ceramics. *Mater. Chem. Phys.*, 1995, **40**, 168–172.
46. Chan, N.-H., Sharma, R. K. and Smyth, D. M., Nonstoichiometry in acceptor-doped BaTiO3. *J. Am. Ceram. Soc.*, 1982, **65**, 167–170.